THE ASTROPHYSICAL JOURNAL, 209:509–524, 1976 October 15

MODEL DUST ENVELOPES AROUND LATE-TYPE STARS

T. W. JONES
National Radio Astronomy Observatory,* Green Bank, West Virginia
AND
K. M. MERRILL
Department of Physics, University of California, San Diego, and School of Physics and Astronomy, University of Minnesota
Received 1976 February 24

ABSTRACT

Spectra have been computed for a large number of spherical model circumstellar dust shells, utilizing realistic grain opacities and assuming steady-state radiative equilibrium around cool stars. Results are shown graphically and the important model parameters evaluated for a wide range of shell optical depths, shell radii, and mass-distribution functions for both silicate and graphite dust grains.

For shells containing silicate grains alone, the 10 μ feature can appear in absorption only when there is considerable optical depth at 10 μ in grains colder than $\sim$250 K. This condition can be relaxed somewhat when other warmer grain species coexist.

A clear-cut distinction exists between models involving "dirty" silicates which effectively absorb at short wavelengths and models involving "clean" silicates mixed with other, more absorptive grains. In the latter case, one must compute a separate energy balance for each grain species, the silicate species generally being much the colder. Results indicate that circumstellar silicate grains probably have greater absorptivities for $1\ \mu \lesssim \lambda \lesssim 5\ \mu$ than terrestrial silicates so far indicate.

Subject headings: infrared: sources — stars: circumstellar shells — stars: late-type

I. INTRODUCTION

The existence of dust grains within the close environment of many late-type stars has been firmly established by extensive observations [see, e.g., Woolf (1973) and Neugebauer, Becklin, and Hyland (1971) for recent reviews]. The presence of such extensive circumstellar dust shells constitutes one of the salient and potentially most informative manifestations of interstellar matter in the condensed state. Frequently thermal dust emission accounts for most of the radiation escaping a star to distant observers, and indeed in many cases the emergent flux has been so altered by passage through the dust shell that the identity of the central radiation source becomes conjectural.

Until recently the complex requirements of all but the simplest models deterred physically realistic treatments of radiation transfer through dense circumstellar dust envelopes. In the past few years, several authors have computed reasonably detailed circumstellar dust-shell models with emphasis placed on spectral fitting of a few individual stars (e.g., Herbig 1970; Apruzese 1974, 1975; Taam and Schwartz 1976). Considering the wealth of detailed observational data available on many stars, one may expect to obtain a greater understanding of the general phenomenon by modeling the characteristics common to a wide range of objects rather than fitting a small and possibly unique subset. This paper summarizes the results of approximately 200 detailed circumstellar dust-shell model calculations in which many of the important physical effects have been accounted for. We emphasize utilization of the observed range of features common to many stellar spectra as a guide to the relevant extent of the model parameter space but make no serious attempt to explain the spectrum of any one specific object. Instead, the paper examines the influence of various model parameters such as shell radius, distribution of material within the shell, optical depth, and grain opacity as well as the influence of scattering and mixtures of distinct grain species. Some of these effects have also been studied in an independent, parallel investigation by Apruzese (1976).

II. THE OBSERVATIONAL PICTURE

Middle-infrared observations of cool stars of known spectral type indicate that the dominant opacity in the circumstellar dust differs for oxygen-rich (M stars) and carbon-rich (C stars) stars (Hackwell 1972; Treffers and Cohen 1974; Forrest, Gillett, and Stein 1975). The strong 10 μ and 20 μ signature characteristic of silicate dust grains appears in M stars, whereas, apart from a resonance feature of silicon carbide (SiC) near 12 μ (which generally contains relatively little energy flux), the infrared continuum

* Operated by Associated Universities, Inc., under contract with the National Science Foundation.

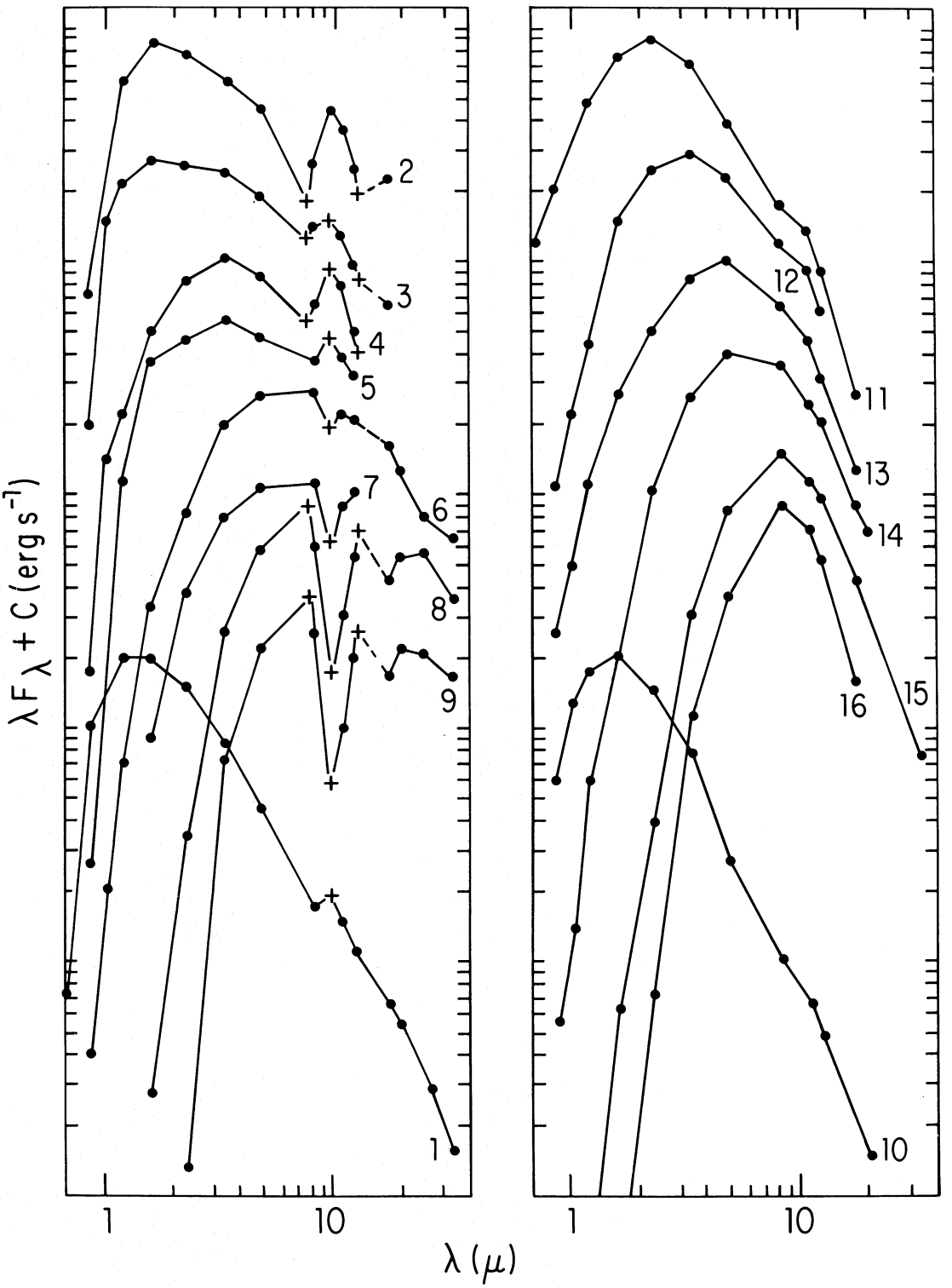

FIG. 1.—Infrared spectra of oxygen-rich (*left*) and carbon-rich (*right*) stars illustrating range of spectral behavior typically observed. Broad bandpass data (dots) and narrow bandpass data (pluses) are from literature as described in text. Sources shown are identified as follows: (1) o Cet, (2) IRC+10322, (3) NML Tau ≡ IRC+10050, (4) WX Ser ≡ IRC+20281, (5) IRC+40004, (6) NML Cyg ≡ IRC+40448, (7) CRL 490, (8) CRL 2591, (9) CRL 2205, (10) UU Aur, (11) R Lep, (12) IRC+40485, (13) IRC+50096, (14) IRC+40540, (15) IRC+10216, and (16) CRL 865. IRC = *Two-Micron Sky Survey* of Neugebauer and Leighton (1969); CRL = *AFCRL Infrared Sky Survey* of Walker and Price (1975).

of C stars is generally featureless and presumed due to graphite.

Figure 1 summarizes the observational picture relevant to this study. The emergent infrared spectra of a number of sources have been selected and arranged to represent a wide range of optical depths in the circumstellar dust shells. Most of the broad bandpass data (dots) between 1.65 μ and 12.5 μ as well as all of the narrow bandpass data at 8 μ, 10 μ, and 13 μ (pluses) are from Merrill (1976), Merrill and Stein (1976), and Forrest, Gillett, and Stein (1975). Other data are taken from Dyck, Lockwood, and Capps (1974); Dyck and Simon (1975); Frogel and Hyland (1972); Hagen, Simon, and Dyck (1975); Humphreys, Strecker, and Ney (1972); Hyland *et al.* (1972); Johnson *et al.* (1966); Lockwood (1970); Low, Rieke, and Armstrong (1973); Morrison and Simon (1973); Simon (1974); Simon and Dyck (1975); Simon, Morrison, and Cruikshank (1972); and Strecker and Ney (1974*a*, *b*).

Note that, for the oxygen-rich stars (Fig. 1, left), there is a trend from net emission (spectra 2–5) to net absorption (spectra 6–9) in the 10 μ silicate feature, whereas, even in the extreme cases CRL 2591 (curve 8) and CRL 2205 (curve 9), evidence of the 20 μ silicate feature remains weak despite deep absorption at 10 μ.

For the carbon-rich stars (Fig. 1, right), the presumed increase of optical depth from spectrum 11 to spectrum 16 results in a gradual increase in the wavelength of peak emission, accompanied by a narrowing of the emergent spectral energy distribution.

Representative central stars with a minimum of obscuring dust (o Cet and UU Aur) are also shown at the bottom of Figure 1.

III. PROCEDURES

a) Solution of the Transfer Equation

The steady-state equation of transfer in spherical geometry was solved numerically using an approximation which consisted in separating the radiation field in each of 17 contiguous wavelength bands (see Table 1) into two components. One component included radiation received directly at a given radius from the central star (the "stellar" field); its intensity was attenuated by a factor $\exp[-\tau_\lambda(r)]$. The second ("diffuse") component, including radiation scattered from the stellar field or produced by thermal emission within the shell was treated in the Eddington approximation; viz., its angular dependence was expanded in Legendre polynomials, only the isotropic and linear terms being kept. The derivation of this and higher-order approximations as well as a discussion of analytic solutions are given in the Appendix.

The procedure above improves upon the standard Eddington approximation in such problems (e.g., Apruzese 1974), since it accounts for variable radiation field anisotropy due to the presence of the central star. Since it cannot account for the anisotropy at outer shell radii due to the finite and nonuniform extent of the shell itself (see, e.g., Hummer and Rybicki 1971; Leung 1975), some inaccuracies remain. However, after these computations were completed, we obtained a copy of a code written by C. M. Leung (Leung 1976) which treats the radiative transfer without approximation. We have rerun several of our models using this code and have found the agreement to be quite good. Even in shells with strong central density concentrations, where one expects our approximations to show most noticeably, the emergent fluxes agreed to better than 5–10 percent when $\lambda \geq 2\ \mu$. In uniform shells the agreement was at least this good everywhere, even in shells of rather large optical depth.

b) Radiative Equilibrium

The equilibrium temperature of a dust-grain species j at a radius r was determined from radiative energy balance:

$$\sum_{i=1}^{17} Q_{\rm abs}{}^{ij} \int_{\Delta\lambda_i} B_\lambda[T_j(r)]d\lambda = \sum_{i=1}^{17} Q_{\rm abs}{}^{ij} \int_{\Delta\lambda_i} J_\lambda(r)d\lambda\,, \tag{1}$$

where B_λ is the Planck function, $Q_{\rm abs}{}^{ij}$ is the absorption efficiency in band i, and the mean intensity, J_λ, includes both the stellar and diffuse fields and is averaged over 4π sr. To improve computing efficiency, the left side of equation (1) was externally fitted piecewise by power laws to better than 1 percent accuracy.

The equilibrium temperature distribution within a shell was found iteratively, beginning with solutions to equation (1) neglecting thermal shell emission. For all but a few models of very large optical depth, temperature convergence to 0.5 percent or better between iterations sufficed to assure conservation of total flux to better than 5 percent and usually better than 1–2 percent, comparable with inherent integration errors in equation (1). Typical model computations required 1–2 min CPU time on the NRAO IBM 360/65.

c) Selection of Grain Parameters

As noted in § II, oxygen-rich stars and carbon-rich stars produce distinctly different infrared spectra due to the different optical properties of the dust grains surrounding them.

Graphite grains were chosen in our model computations to represent the dominant source of opacity in shells surrounding carbon-rich stars. Although SiC grains seem to be present, they should have little distinctive influence outside the narrow $\sim 12\ \mu$ resonance and can safely be neglected for calculations at the present level of sophistication. Graphite opacities between 0.3 μ and 30 μ were calculated using Mie theory for spherical grains of radius $a = 0.05\ \mu$ (a typically quoted value; see, e.g., Salpeter 1974*a*) and optical constants from Taft and Philipp (1965) for monocrystalline graphite with the electric vector in the basal plane. For $\lambda > 30\ \mu$, $Q \propto \lambda^{-2}$, appropriate

1976ApJ...209..509J

TABLE 1

GRAIN OPACITIES

BAND	λ (μ)	$\Delta\lambda$ (μ)	GRAPHITE [Q_{ext} ($\tau/\tau_{10\,\mu}$)]	(a = 0.05 μ) Albedo	(a = 0.05 μ) Phase Factor	DIRTY SILICATE [Q_{ext} ($\tau/\tau_{10\,\mu}$)]	(a = 0.1 μ) Albedo	(a = 0.1 μ) Phase Factor	CLEAN SILICATE [Q_{ext} ($\tau/\tau_{10\,\mu}$)]	(a = 0.1 μ) Albedo	(a = 0.1 μ) Phase Factor
1	0.45	0.3	1.83 (306)	0.3	0.11	1.18 (12.9)	0.6	0.55	0.529 (5.83)	0.99	0.46
2	0.75	0.3	0.628 (105)	0.12	0.04	0.355 (3.91)	0.38	0.4	0.123 (1.36)	0.98	0.13
3	1.05	0.3	0.332 (55.5)	0.06	0.02	0.177 (1.95)	0.21	0.23	0.0328 (0.361)	0.93	0.07
4	1.5	0.6	0.162 (27.1)	0.031	0.01	0.099 (1.1)	0.095	0.09	0.01 (0.11)	0.79	0.03
5	2.3	1.0	0.0733 (12.3)	0.013	...	0.0577 (0.636)	0.03	0.01	0.00316 (0.0348)	0.45	0.015
6	3.4	1.2	0.038 (6.36)	...	...	0.036 (0.397)	...	...	0.0017 (0.0187)	0.15	...
7	4.9	1.8	0.02 (3.41)	...	...	0.0248 (0.273)	...	...	0.00195 (0.0215)	0.037	...
8	6.8	2.0	0.0115 (1.92)	...	...	0.02 (0.22)	...	...	0.0113 (0.124)	...	...
9	8.4	1.2	0.0079 (1.32)	...	...	0.0468 (0.515)	...	...	0.0468 (0.515)	...	...
10	9.9	1.8	0.00598 (1.00)	...	...	0.0908 (1.00)	...	...	0.0908 (1.00)	...	...
11	11.9	2.2	0.00429 (0.717)	...	...	0.05 (0.551)	...	...	0.05 (0.551)	...	...
12	14.5	3.0	0.00292 (0.488)	...	...	0.0227 (0.25)	...	...	0.227 (0.25)	...	...
13	20.0	8.0	0.00128 (0.214)	...	...	0.0458 (0.504)	...	...	0.0458 (0.504)	...	...
14	27.0	6.0	0.00057 (0.0953)	...	...	0.0423 (0.466)	...	...	0.0423 (0.466)	...	...
15	40.0	20.0	0.00024 (0.040)	...	...	0.00659 (0.0726)	...	...	0.00659 (0.0726)	...	...
16	100.0	100.0	4.8×10^{-5} (0.008)	...	...	0.00031 (0.0034)	...	...	0.00031 (0.0034)	...	...
17	350.0	400.0	4.4×10^{-6} (0.00074)	...	...	0.000028 (0.00031)	...	...	0.000028 (0.00031)	...	...

to small particles, was assumed (Andriesse 1974; Aannestad 1975). Assumed optical properties of graphite are listed in Table 1.

Shells surrounding M stars apparently consist in part of silicate grains. Since the observed characteristics of the 10 μ and 20 μ features are rather smooth and similar from source to source (see, e.g., Treffers and Cohen 1973; Forrest, Gillett, and Stein 1975) in comparison with results expected from laboratory-measured optical constants (see, e.g., Aannestad 1975), we have followed Gillett, Forrest, *et al.* (1975) in modeling the two features after the observed 10 μ emission profile of the Trapezium region of Orion (corrected for an assumed 250 K temperature).

Model silicate grains were assumed to have radii $a = 0.1\ \mu$ (see, e.g., Salpeter 1974*a*). The feature peaking at 9.7 μ was normalized to give the same integrated band strength as features in representative terrestrial silicates (Pollack, Toon, and Khare 1973). The other band was assumed to peak at 22 μ and to have the same shape, but 0.7 of the integrated strength, of the 9.7 μ band.[1] For $\lambda > 50\ \mu$; a $Q \propto \lambda^{-2}$ dependence was assumed.

Short of 8 μ two distinctly different model silicate opacities were investigated. The first material was assumed to have the optical constants of basaltic rock (Pollack, Toon, and Khare 1973). The resulting optical properties are given in Table 1. These grains produce relatively little absorption in the 1–5 μ range, where for our models most of the stellar flux emerges (hence we will refer to them as "clean" silicates). In model calculations such grains remain rather cold even relatively near the central star; hence very large 10 μ optical depths ($\gg 1$) are required before a significant fraction of the stellar energy flux is reradiated by the silicate dust. This conflicts strongly with the appearance of actual spectra such as those of Figure 1 (left).

Consequently, we have calculated models using a "dirty" silicate with an index of refraction for $\lambda < 8\ \mu$ assumed to be $m = 1.55 - 0.1i$, roughly consistent with values reported for the matrix material meteoric rock (Dorschner 1968, 1971*b*). Such dirty grains could result, for example, from surface or lattice contamination. The optical properties of these grains are also given in Table 1. Model spectra computed using these grains were in significantly better agreement with observation, and these opacities incidentally produced good agreement with the observed infrared extinction in front of the star VI Cyg #12 (Gillett, Jones, *et al.* 1975).

As an alternative to dirty silicate grains, we considered mixtures of the clean silicate grains and graphite grains (taken to represent behavior of various metallic grains). As we will discuss in some detail later, even when the net opacities of such mixtures match the opacities of the dirty silicates, the resulting models are significantly different.

[1] These choices are roughly consistent with values found for carbonaceous chondrites (Zaikowski and Knacke 1975) and lunar rock (Knacke and Thomson 1973). Although the relative strength and position of the 20 μ band are important in matching models to observations, the basic character of the present models is insensitive to such details.

d) Stellar and Shell Parameters

Within the assumption of spherical symmetry, we show in the Appendix that solutions of the transfer-radiative equilibrium equations require specification of only a small number of rather general characteristics of the star and surrounding shell. For example, one need not specify independently the stellar luminosity L_* and shell outer radius R, but solutions can be uniquely determined, even for optically thick shells, by the fluxlike parameter $\mathfrak{F} \equiv L_*/R^2 \equiv 4\pi\sigma T_e^4 (r_*/R)^2$, where r_* is the stellar radius. (As mentioned below, one must, of course, further specify the ratio of shell inner and outer radii.) This parameterization is particularly useful, since observationally one measures flux and angular size. A measured angular scale θ can be related to a normalized shell-model radius $\rho = r/R$ through the relation $\rho = \theta[\mathfrak{F}/(4\pi F)]^{1/2}$, where F is the observed wavelength-integrated flux; *thus model and source can be compared without knowledge of source distance or luminosity.* We have considered a wide range of the parameter $\mathfrak{F}$.

Additionally, one must assume a shape for the stellar continuum. We have for all the models discussed here taken this shape to be that of a 2400 K blackbody, since many isolated compact infrared sources appear otherwise to be normal cool stars (Merrill 1976; Merrill and Stein 1976; Strecker and Ney 1974*a*, 1974*b*; Dyck, Lockwood, and Capps 1974; Lockwood 1974; Vogt 1973), and this temperature is consistent with the spectra of o Ceti and UU Aur shown in Figure 1. With T_e equal to the same (color) temperature, the ratio r_*/R then becomes fixed by the parameter $\mathfrak{F}$. Scaling results to different stellar temperatures is not simple but physically is much the same as altering the opacity wavelength dependence, which is briefly discussed in § IV*d*.

To solve the transfer equation, one must specify $\rho_i = r_i/R$, where r_i is the inner radius of the dust shell. Since the dust grains in these circumstellar shells probably condense in the stellar atmosphere, it would be most realistic to limit the inner shell radius according to the temperature at which a given grain species condenses. Since this radius depends upon the solution itself and somewhat upon the other variable model parameters, we have chosen the comparable but simpler procedure of fixing the ratio $r_i/r_* = \rho_i/(4\pi\sigma T_e^4 \mathfrak{F})^{1/2}$ at values $r_i/r_* \approx 4$ for dirty silicates and $r_i/r_* \approx 1.6$ for graphite and clean silicates, assuring for all models that the silicate (graphite) temperatures not exceed their likely condensation temperature $\sim$1200 K ($\sim$1700 K) (Gilman 1969; Salpeter 1974*a*).

Finally, one must specify at each radius the function $[d\tau_\lambda(\rho)]/(d\rho)$ along with the effective scattering albedo and scattering pattern (represented to lowest order by g, the phase parameter) at each wavelength. [As indicated earlier, one must also specify $Q_{\rm abs}(\lambda)$ for each grain species, in order to solve the equation of

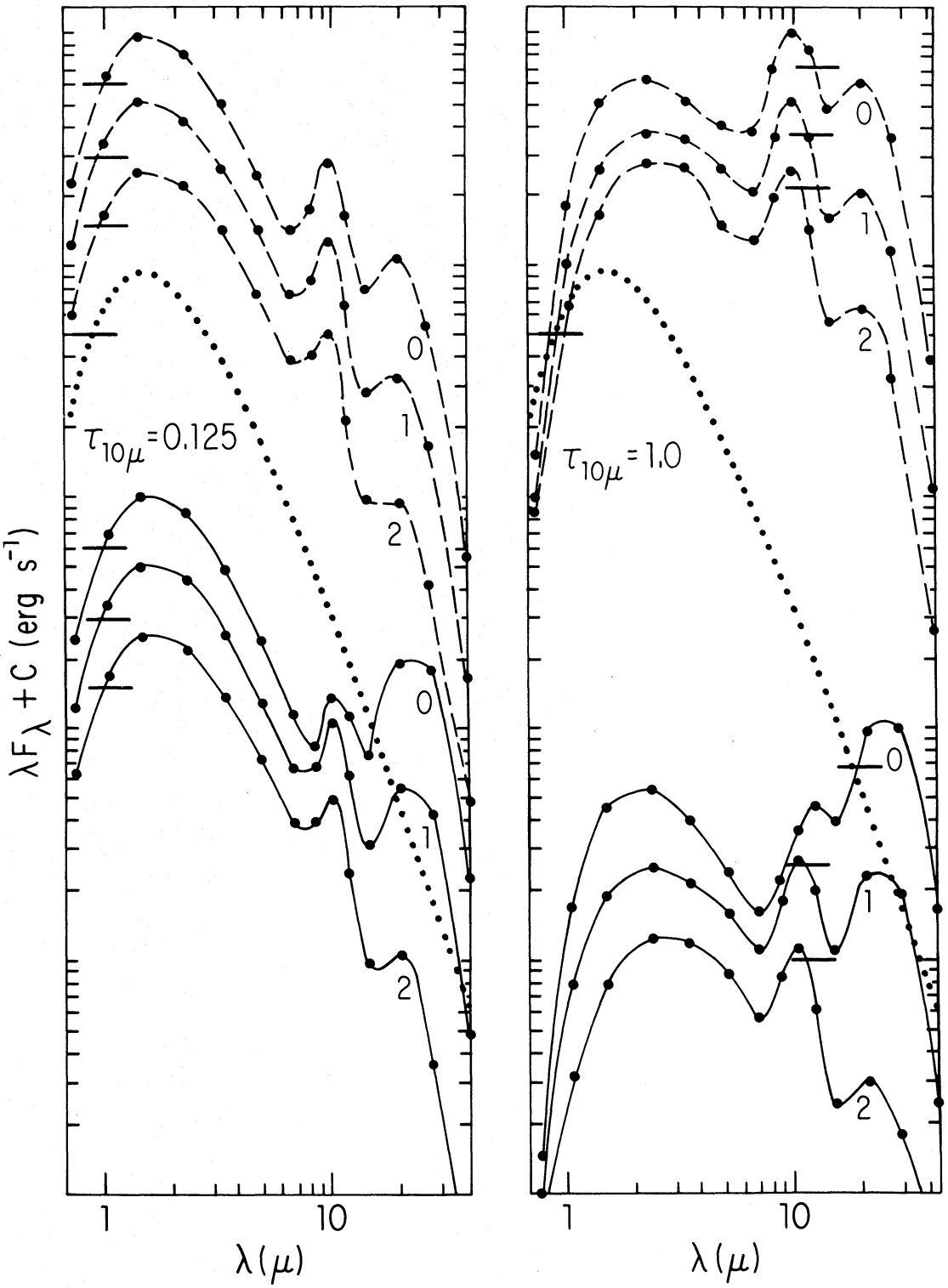

FIG. 2*a–d*.—Model emergent spectra (star plus shell) calculated for "dirty" silicate shells. Dotted curve is spectrum of underlying 2400 K star. Spectra have arbitrary relative vertical placements, but each contains a horizontal bar at $\lambda F_\lambda = 5 \times 10^{37}$ ergs s^{-1} (here —F_λ represents flux integrated over shell surface, and total luminosity is assumed to be $L_* = 3.25 \times 10^4 L$). Any two spectra may be compared in detail using a pair of dividers and this reference. Dashed curves represent spectra for shells of radius $R = 6 \times 10^{15}$ cm ($R/r_* = 80$), while solid curves represent results for shell radii 5 times larger. Each curve is labeled by index α of assumed grain density distribution function ($n \propto r^{-\alpha}$).

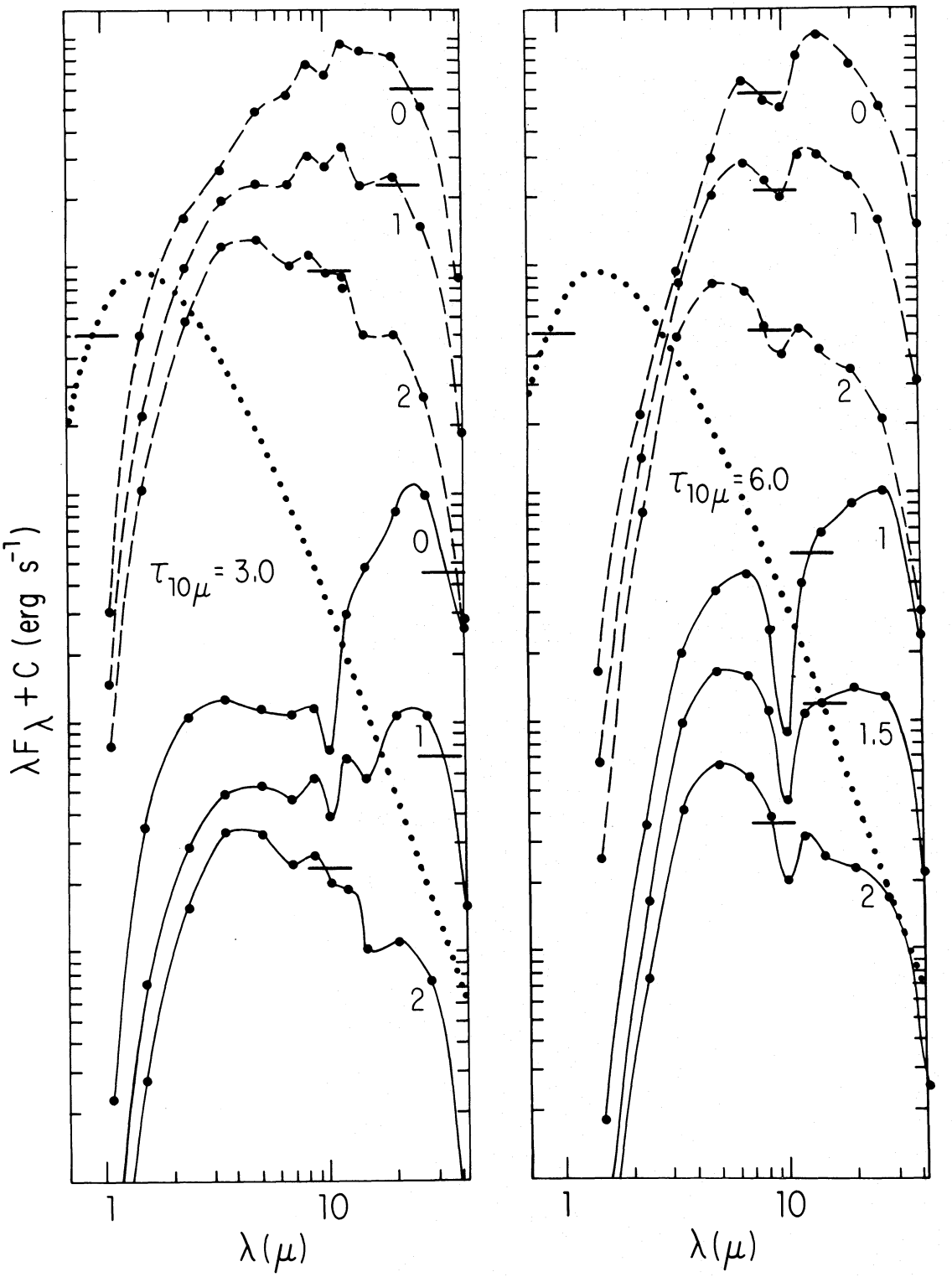

FIG. 2.—*Continued*

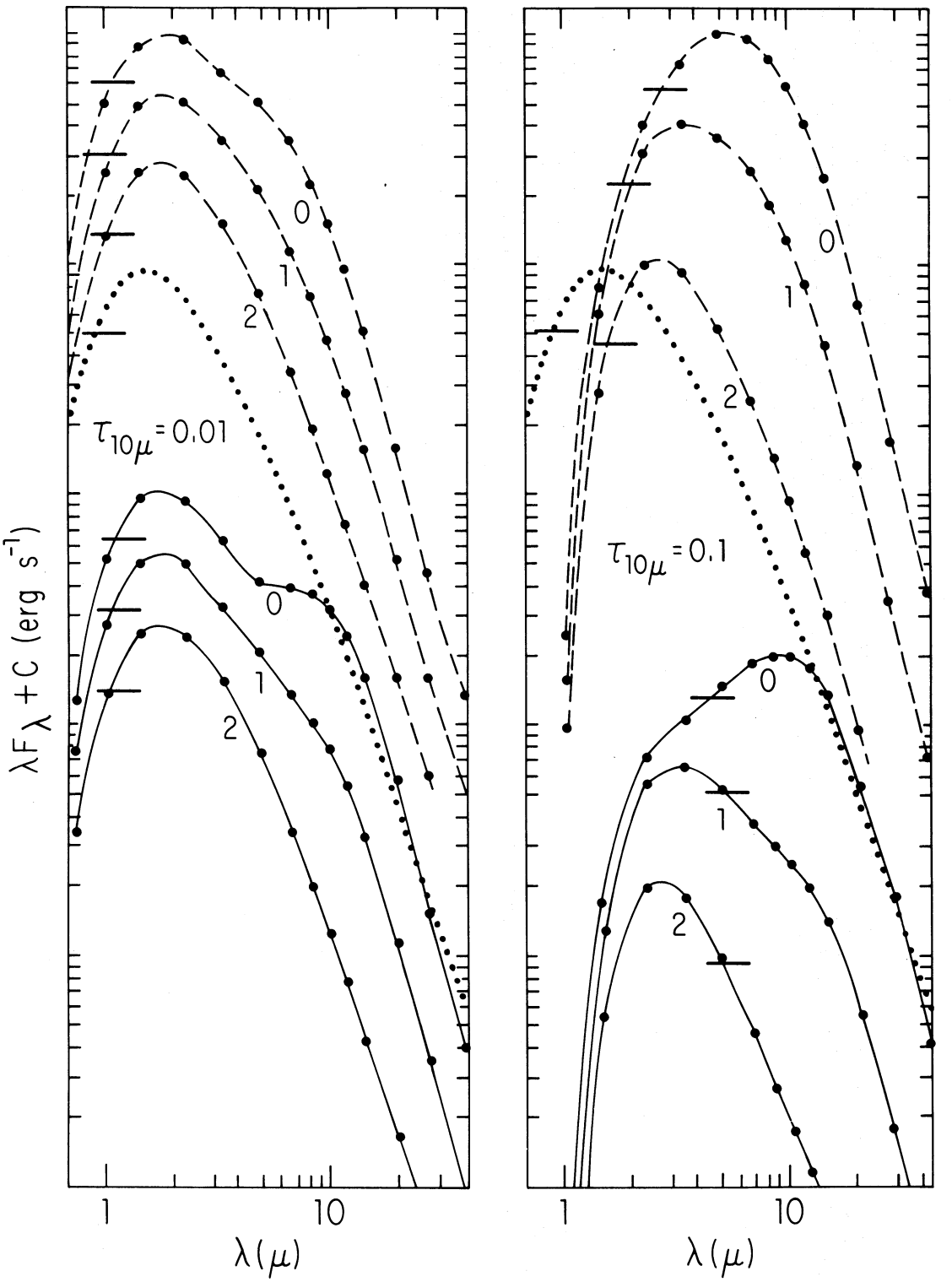

FIG. 2*e–h*.—Same as Fig. 2*a–d*, except for graphite shells. In this case larger shells have radii 4 times smaller ones.

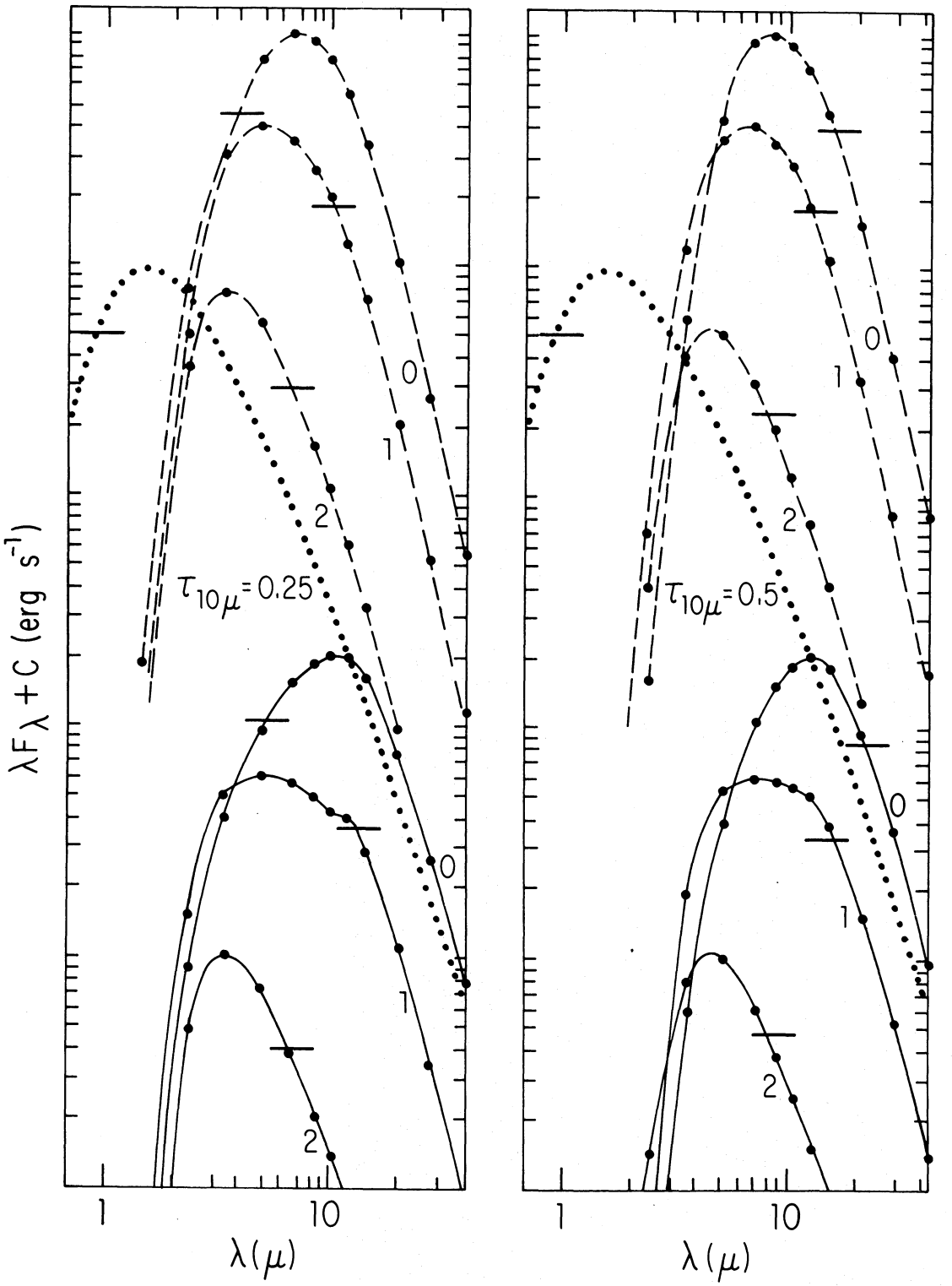

FIG. 2.—*Continued*

radiative equilibrium.] In most models we have assumed a form

$$\frac{d\tau_\lambda}{d\rho} \propto \rho^{-\alpha} \quad (\rho_i \leq \rho \leq 1), \tag{2}$$

with the subsidiary information (e.g., albedo) determined by weighted optical properties of the grain species present. Values of α near 2 are of special interest, since steady radiation-pressure-driven flows in optically thin shells approach this form (Gilman 1972; Salpeter 1974*b*; Kwok 1975).

IV. RESULTS

Although it was emphasized in the previous section that one need not specify the luminosity of a model star to compare the model with observation, it is somewhat simpler to understand the effects of various physical parameters if one discusses them for a single model star. We shall therefore discuss our results in terms of a late-type supergiant star with luminosity $L_* = 3.25 \times 10^4 L_\odot (M_{\rm bol} = -6.5)$. Figures 2*a*–2*h* illustrate the range of behavior found for model dirty silicate and graphite emergent (total) spectra. Spectral information beyond 40 μ has been omitted, since for the cases considered such fluxes were always relatively small and qualitatively easy to predict from the other data. Because of the sensitivity of the emergent optical fluxes to uncertainties in opacity, albedo, and geometry, we have also omitted the 0.45 μ fluxes as well as those at somewhat longer wavelengths when they are small. Because the 10 μ silicate feature is of prime interest, we have referenced the optical depth to this wavelength, but values at any wavelength can be found using Table 1. Emphasizing again that our aim has not been to fit individual source spectra, we note in comparing Figures 1 and 2 that most of the observed spectra in Figure 1 resemble in some measure one or more of the model spectra in Figure 2 (or what one can infer to result from parameter interpolation).

We follow with summaries of the influence of important shell and grain parameters on emergent model spectra:

a) Outer Shell Radius

The shell radius R (or equivalently the parameter $\mathfrak{F}$) is perhaps the simplest parameter to understand, since grain temperatures are largely determined by the degree of radiation dilution. The grain temperatures in turn determine emission at a given wavelength and, in narrow features, a grain's effectiveness in absorption against warmer interior dust. Figure 2 shows, over a range of optical depths and distributions of shell material, the emergent spectra for $R = 6 \times 10^{15}$ cm ($R/r_* = 80$, $\mathfrak{F} = 3.6 \times 10^6$ ergs cm^{-2} s^{-1}). Also shown for silicate shells are $R = 3 \times 10^{16}$ cm ($R/r_* = 400$, $\mathfrak{F} = 1.4 \times 10^5$ ergs cm^{-2} s^{-1}) and, for graphite shells, $R = 2.4 \times 10^{16}$ cm ($R/r_* = 320$, $\mathfrak{F} = 2.3 \times 10^5$ ergs cm^{-2} s^{-1}).

b) Distribution of Grains

Since the grain distribution [eq. (2)] may be weighted toward the inside or outside of the shell, α[eq. (2)] in part plays the same role as R. Figure 2 illustrates for each of several optical depths and shell radii the spectral dependence on α.

No results for $\alpha < 0$ have been plotted; to a first approximation, such spectra resemble those with $\alpha = 0$, because mass and optical depth are concentrated in roughly the same (outer) portions of the shell (see also Apruzese 1976).

The increased fraction of shell material at small radii for $\alpha > 0$ models results in a higher characteristic grain temperature and a shorter wavelength of peak emission. When the optical depth in the 10 μ and 20 μ silicate features is large, the same effect reduces the apparent absorption depth of the 10 μ feature. Note that, when $\alpha = 2$, the spectra are insensitive to $R(\mathfrak{F})$; r_i/r_* is then the more important parameter.

The apparent size of a source will generally be much smaller than R, particularly when $\alpha > 0$. Although our standard transfer procedure does not allow determination of the emergent angular distribution of radiation, we have calculated the emergent infrared intensity distribution for a few models, using a ray-tracing technique and grain temperatures borrowed from our standard solutions. Generally, most of the emergent spectral flux at a given wavelength λ appears to originate well inside the radius at which the grain temperature equals the Wien's displacement law temperature $T_w \approx 3000/\lambda(\mu)$. Figure 3 illustrates the radial temperature dependence over a range of α and optical depth for several dirty silicate and graphite shell models.

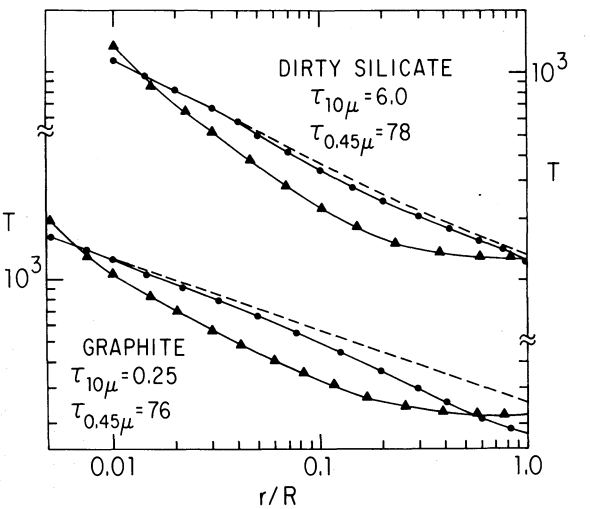

FIG. 3.—Temperature distribution in several model dirty silicate and graphite shells. Shell radius in each case is $R = 2.4 \times 10^{16}$ cm. Dashed curves show temperatures in limit of zero optical depth. Other two curves for each grain species show temperature distribution for model optical depth shown and for uniform dust density (circles) and r^{-2} density dependence (triangles).

c) *Optical Depth*

i) *Effect on Grain Temperatures*

Both the absorption and scattering optical depths as well as their distribution in radius play important roles in the determination of shell temperature structure.

When scattering optical depths at short wavelengths are large, photon transport at these wavelengths is diffusive. Especially at small radii and when $\alpha > 0$, the resulting reduction in photon escape rates enhances their density and increases grain heating. When absorption optical depths are large at wavelengths as long as a few microns, total energy transport is diffusive at small radii, with similar results. This tendency for hotter grains at small radii when $\alpha > 0$ can be seen in Figure 3.

In the outer portions of thick shells, grains are heated primarily by radiation from other grains rather than the more highly obscured star, and, since this radiation peaks at longer wavelengths where the grains absorb relatively poorly (except in the 10 μ and 20 μ silicate bands) the grains tend to be cooler than in thin shells (see Fig. 3).

ii) *Obscuration of the Inner Shell*

Shell optical depth, its radial distribution, and the opacity wavelength dependence control those portions of the shell "seen" by the outside observer, thereby influencing the shape of the emergent spectrum.

Since such effects are simpler for monotonic opacity, we discuss the results first for graphite. Details of the 10 μ and 20 μ silicate features are discussed below. In shells which are optically thick at near-infrared wavelengths, a larger portion of the inner cloud is obscured at shorter wavelengths. To a certain extent, the peak wavelength of the emergent spectrum in optically thick shells is influenced by this effect. The result is simplest for $\alpha = 2$, when the Wien's displacement law temperature of the spectral peak generally corresponds to the grain temperature roughly unit optical depth into the shell at the peak wavelength. Thus, with increasing optical depth, the peak wavelength increases, because only the cooler dust (radiating at longer wavelengths as well as farther out) is visible from the outside. This effect is accentuated by the influence of optical depth on grain temperatures but would clearly occur anyway. Similarly, the increasing opacity toward shorter wavelengths results in a spectral shape at wavelengths less than the peak, generally steeper than a single blackbody. Further, a flattening (steepening) in the wavelength dependence of the opacity would tend to make the spectrum broader (narrower) because of changes in the observable temperature range.

It may be worth noting that the wavelength peak and the width of spectra for models with $\alpha = 2$ are quite sensitive to changes in r_i/r_* or to deviations from the power-law form. Thus really meaningful models of this sort will require detailed dynamical models for the shells as well. For example, our preliminary attempts at extending radiation-pressure-driven mass-loss models to optically thick shells suggest that the mass-loss rates will be significantly reduced and that the grain distribution will be flattened at small shell radii from the $n \sim r^{-2}$ optically thin solutions (Kwok 1975).

iii) *Spectral Shape at Optically Thin Wavelengths*

When $\alpha < 2$ and especially when R is large, there appears a "knee" in the spectrum at optically thin wavelengths beyond the peak described above (see Figs. 2*e*–2*h*). The Wien's displacement law temperatures of this knee correspond roughly to grains at $\frac{1}{4}$–$\frac{1}{2}$ the shell radius depending upon α but being almost independent of optical depth.

Similarly, the color temperature of the 10 μ and 20 μ silicate features, when corrected for their different emission strengths, generally corresponds (as long as $\tau_{10\mu} < 1$) to grain temperatures at radii from $r/r_i \sim 6(\alpha = 2)$ to $r/R \sim 0.4(\alpha = 0)$. As the near-infrared optical depth becomes larger, the long wavelength knee (and for silicates the 10 μ and 20 μ features) develops into the dominant spectral peak.

iv) *The Silicate Features: Emission or Absorption*

When the optical depth of silicate dust shells becomes large at 10 μ, this feature may appear in absorption. Since this occurs both in model and real spectra and since the appearance of this feature is frequently used to estimate shell optical depth, the transition from emission to absorption is important to understand. In principle, the 20 μ feature may also be in absorption, but limited data available to date do not unambiguously show this.

In spherically symmetric shells containing silicate grains only, a large optical depth ($\gtrsim 1$) at 10 μ in dust colder than $T_w \sim 250$ K is ordinarily required to produce the 10 μ feature significantly in absorption. This may be seen by the following simple argument:

If, upon integrating inward at wavelength λ, the shell becomes opaque at radius r_0, then in the first approximation the emergent flux is $\lambda F_\lambda \propto r_0^2 \lambda B_\lambda [T(r_0)]$. If $T(r_0) > T_w$, with T_w the Wien's displacement law temperature, $\lambda B_\lambda \sim T/\lambda^3$. Assuming for simplicity $T \propto r_0^{-1/2}$, then $\lambda F_\lambda \sim T^{-3}$. Consequently, since T is smallest at the band center (r_0 is largest), the feature should appear in emission. Conversely, if $T(r_0) < T_w$, $\lambda F_\lambda \propto r_0^2 \lambda^{-4} \exp [(-hc)/(\lambda T)] \sim T^{-4} \exp (-5\, T_w/T)$. Since, in the designated range, this form gives $(d\lambda F_\lambda)/(dT) > 0$, the feature should appear in absorption. Our detailed calculations confirm that only the opacity in dust with $T < T_w$ is capable of producing the 10 μ feature in absorption. A similar analysis applies to the 20 μ feature, for which $T_w \sim 125$ K. Thus, when the 10 μ feature appears in absorption, the emergent spectral form in the 20 μ feature (i.e., emission vs. absorption) depends on the relative intrinsic strengths of the two features and the fraction of total optical depth at large radii.

If another species of hotter grains coexists with the silicates [see § IV*d*], more detailed considerations are necessary, but generally the silicate features can appear in absorption for somewhat smaller optical depths and higher temperatures (see Fig. 4*b*).

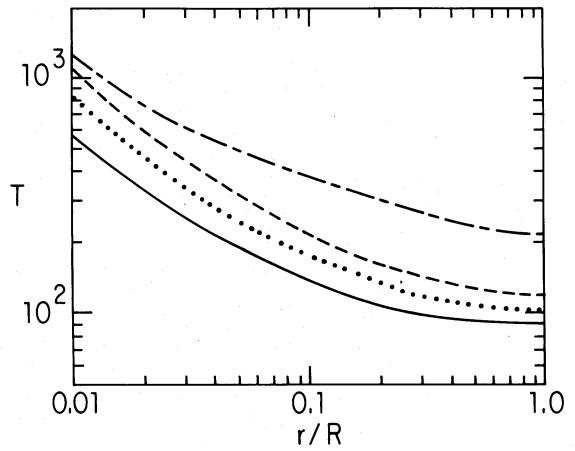

FIG. 4*a*.—Comparison of temperature distributions in models using dirty silicates (dashed curve) and a 40/60 by number clean silicate/graphite grain mixture having approximately the same net optical characteristics (with $R = 3 \times 10^{16}$ cm, $\alpha = 2$, and $\tau_{10\mu} = 2.0$). Clean silicate temperatures are indicated by solid curve and graphite by dot-dashed curves. Also shown (dots) (for same shell parameters) is temperature distribution for silicate component when $Q_{abs} = 0.01$ for $\lambda \leq 5\ \mu$.

We note in passing that the possibility of an emission feature at 20 μ in conjunction with an absorption feature at 10 μ in circumstellar spectra contrasts sharply with the absorption features at both wavelengths expected for general interstellar extinction (due to cold dust distributed along the line of sight).

v) *Importance of Scattering to These Models*

To evaluate the importance of scattering to the model spectra, we computed several models in which scattering was suppressed. The flux changes were substantial at short wavelengths, partly due to drops as large as 10 percent in the grain temperatures near the star. But for $\lambda > 2\ \mu$, the emergent fluxes were never changed by more than 10 percent from the corresponding model with scattering included (largest changes were in clean silicate models). This insensitivity results from the small grains and cool stellar source functions used in these calculations. Most of the stellar flux occurs at wavelengths where scattering is not a dominant effect. Scattering would play a more significant role in models utilizing hotter stars and/or larger grains.

We also computed several models in which the anisotropy of grain scattering was ignored, with no significant changes in the emergent spectral fluxes for $\lambda > 1\ \mu$. Taam and Schwartz (1976) found this effect to be much more important in their models of VY CMa, primarily because they used rather large dust grains ($\bar{a} = 0.5\ \mu$) which scatter more effectively for $\lambda \geq 1\ \mu$.

d) Grain Mixtures

As an alternative to dirty silicates and to study the relative importance of individual grain and bulk opacities, we considered shells composed of a mixture of clean silicate and graphite grains [see § III*d*]. A mixture containing 40 percent by number of clean silicate grains reproduced to a good approximation the optical properties of the dirty silicates in Table 1. In contrast to previous models involving grain mixtures (e.g., Taam and Schwartz 1976), we computed the radiative energy balance separately for each grain species, allowing each to come to its own equilibrium temperature. Figure 4*a* compares for one set of shell parameters the temperature distribution of dirty silicate grains with those of the clean silicate and graphite grains in this mixture.

Because the clean silicate grains are rather cold, they

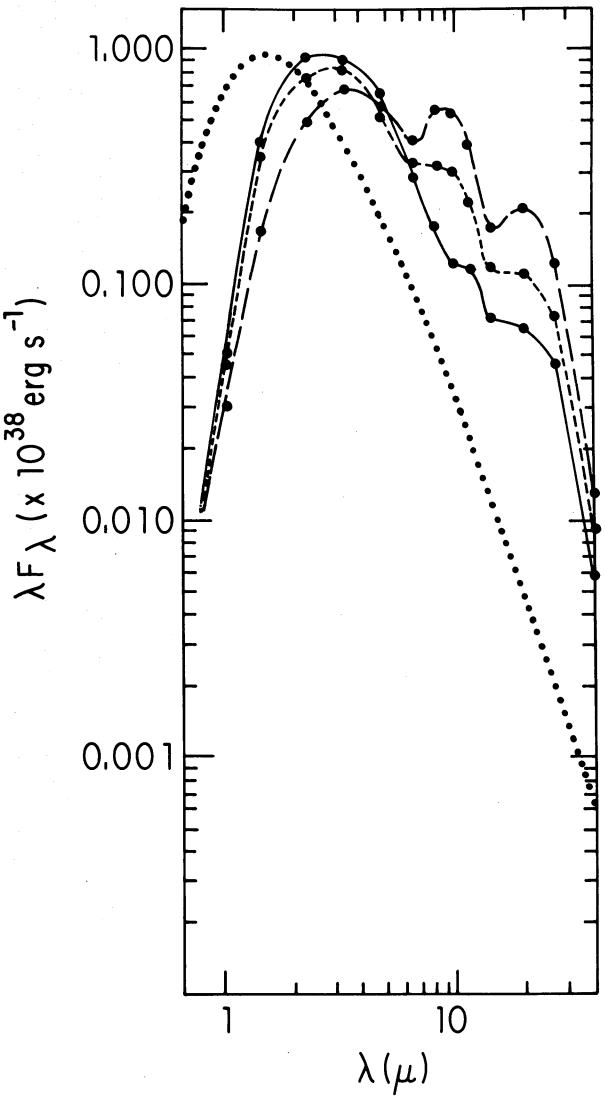

FIG. 4*b*.—Spectra resulting from the models described in Fig. 4*a*. Long-dash curve represents spectrum in dirty silicate model; solid curve is that for first grain mixture, short-dash curve for second mixture.

are usually poor emitters at 10 μ and 20 μ and tend, instead, to absorb (especially at 10 μ) against the emission of the much hotter graphite grains (see Fig. 4*b*). We were unable to find any model involving the basaltic (clean) silicate-graphite mixtures capable of producing 10 μ and 20 μ emission features like those seen in Figure 1 (left). Largely, this is a consequence of the poor absorption by silicates in the 1–5 μ range. To demonstrate this, we calculated several identical grain-mixture models, except that now the silicate absorption efficiency was set to the value $Q_{\rm abs} = 0.01$ for $\lambda \leq 5\,\mu$, an increase of factors between 2 and 5 over the basaltic values in this range. The resulting silicate temperature distribution for the comparable model is also shown in Figure 4*a*, and the spectrum in Figure 4*b*. The silicate features are in this model significantly stronger than for basaltic silicates but still rather weak in comparison with typical observed strengths.

It is clearly important, therefore, to establish in shells containing silicates the short-wavelength absorptivities of the silicate grains themselves, not just the net absorptive opacity of all the grains present. Furthermore, it is important to consider that different species will come to different equilibrium temperatures. Moreover, based on these results, we conclude that circumstellar silicate grains are likely to be "dirtier" than terrestrial silicate minerals seem to be and that silicate grains themselves probably absorb directly a significant fraction of the energy taken from the stellar flux.

V. CONCLUSIONS

Finally, we single out several of our more important findings:

1) Spherical-model circumstellar dust shells composed only of "clean," i.e., poorly absorbing, silicate grains with radii $a \sim 0.1\,\mu$ do not produce spectra like those observed. This is because the silicate grains absorb little of the stellar energy unless they are very opaque in the 10 μ and 20 μ features (contrary to observation).

2) The difficulty above remains when distinct, more highly absorbing grains are mixed in, so we conclude that circumstellar silicate grains are at least moderately good absorbers of visual and near-infrared radiation. Shells made of "dirty" silicate grains seem to be able to produce spectra similar to those actually observed.

3) To calculate model spectra, it is insufficient, when several grain species are present, to use only the net optical characteristics of the mixture to calculate the radiative equilibrium of the grains. One must allow each grain species to reach its own equilibrium temperature. The sensitivity of emergent spectra to individual rather than net opacity potentially provides additional information about the grains not available from general interstellar extinction in the infrared (where only the net opacity can be inferred).

4) Spherical shells containing silicate grains alone will show the 10 μ feature in absorption only when dust cooler than $\sim$250 K is itself opaque. Thus the total 10 μ optical depth generally will significantly exceed that implied directly by the measured absorption depth. The appearance at 10 μ of an absorption feature does not in itself imply one at 20 μ. Shells containing silicate grains mixed with metallic grains, which tend to be hotter, are more prone to showing the 10 μ feature in absorption.

5) Computation of the angular distribution of the emergent fluxes and computations with higher-wavelength resolution, to match, for example, available spectrophotometry in the silicate bands, should allow a more quantitative description of the circumstellar dust envelopes of individual sources (allowing determination, e.g., of individual shell masses and mass-loss rates).

6) Since the emergent spectral information depends rather strongly upon the assumed details of the shell structure, dynamical calculations of shells (including, e.g., the effects of optical depth on radiation pressure) are needed for self-consistent solutions.

We gratefully acknowledge useful discussions with C. M. Leung, B. T. Soifer, and W. A. Stein. This work has been supported in part at the University of California, San Diego, and the University of Minnesota by the National Science Foundation.

APPENDIX

SOLUTION OF THE TRANSFER EQUATION

I. GENERAL PROCEDURE

In a spherically symmetric source containing dust and, for generality, gas, the equation for transfer of specific intensity $I_\lambda(\theta, r)$ takes the form

$$\mu \frac{\partial I_\lambda}{\partial r} + \frac{1-\mu^2}{r}\frac{\partial I_\lambda}{\partial \mu} = \epsilon_\lambda - \kappa_\lambda I_\lambda + \frac{1}{4\pi}\tilde{\omega}_\lambda \kappa_{\lambda d}\int_{-1}^{1}\int_{0}^{2\pi} P_\lambda(\gamma) I_\lambda(\mu')\, d\mu'\, d\phi' \,, \tag{A.1}$$

where $\mu = \cos\theta$, $\kappa_\lambda = \kappa_{\lambda d} + \kappa_{\lambda g}$ is the total opacity due to dust and gas, ϵ_λ is the emissivity (assumed isotropic),

$\tilde{\omega}_\lambda$ is the dust albedo, and $P_\lambda(\gamma)$ is the scattering phase function (cf., e.g., Chandrasekhar 1960). Expanding the phase function in Legendre polynomials, so that

$$P(\gamma) = \sum_{j=0}^{\infty} p_j P_j(\cos\gamma),$$

and the intensity in the form

$$I_\lambda(\mu, r) = I_{\lambda d} + I_{\lambda *} \approx \sum_{j=0}^{\infty} K_{\lambda j}(r) P_j(\mu) + \frac{1}{2\pi}\frac{L_* f_\lambda}{4\pi r^2} e^{-\tau}\delta(1-\mu),$$

where the last term accounts approximately for the presence of a central star of specific luminosity $L_* f_\lambda$, τ_λ being the extinction optical depth from the star at radius r, then equation (A.1) becomes (cf. Dorschner 1971*a*)

$$\tfrac{1}{3}K_1' + \frac{2}{3}\frac{1}{r}K_1 + \sum_{j=1}^{\infty} P_j\left[\left[\frac{j}{2j-1}K'_{j-1} + \frac{j+1}{2j+3}K'_{j+1} + \frac{1}{r}\left\{K_{j+1}\left[\frac{(j+1)(j+2)}{2j+3}\right] - K_{j-1}\frac{j(j-1)}{2j-1}\right\}\right]\right] \tag{A.2}$$

$$= \epsilon - \kappa\sum_{j=0}^{\infty} P_j K_j + \tilde{\omega}\kappa_d \sum_{j=0}^{\infty} P_j p_j\left(\frac{1}{2j+1}K_j + \frac{1}{4\pi}\frac{L_* f}{4\pi r^2}e^{-\tau}\right).$$

(For simplicity the functional dependences have been suppressed, and the primes indicate differentiation with respect to r.)[2]

Utilizing the linear independence of Legendre polynomials and transforming to a new set of dimensionless quantities, equation (A.2) can be written as the infinite set of equations

$$S_1' = 3\left(\rho^2\eta - \rho\zeta_0 S_0 + \frac{\tilde{\omega}}{4\pi}\zeta_d S_*\right) \tag{A.3a}$$

$$\frac{j+1}{2j+3}S'_{j+1} + \frac{j}{2j-1}\rho^2 S'_{j-1} = j\rho S_{j-1} - \zeta_j S_j + \frac{\zeta_d p_j \tilde{\omega}}{4\pi}\rho^j S_*(j \geq 1), \tag{A.3b}$$

$$\tau' = \zeta = \zeta_g + \zeta_d \tag{A.3c}$$

with

$$\begin{aligned} \rho &= r/R, \\ S_j &= \rho^{j+1}(K_j/\mathfrak{F}), \\ \mathfrak{F} &= L_*/R^2, \\ S_* &= fe^{-\tau}/(4\pi), \\ \zeta &= \kappa R, \\ \zeta_j &= \zeta_g + \hat{\phi}_j\zeta_d, \\ \hat{\phi}_j &= 1 - \frac{\tilde{\omega}p_j}{2j+1}, \\ \eta &= \epsilon R/\mathfrak{F}, \end{aligned} \tag{A.3d}$$

and R = the outer source radius. Note that, for dust shells in radiative equilibrium around a central star, $\eta = [\zeta_0 B(T)]/\mathfrak{F}$. Since the Planck function B depends itself upon η throughout the source, the equations of (A.3) are nonlinear. But, by considering the iterative solution, initially setting $\eta = 0$, one can readily see that the final solution depends upon L_* and R only through the parameter $\mathfrak{F}$. [The solution, of course, depends further upon boundary conditions such as eq. (A.5).]

In principle, one can solve equation (A.3) to arbitrary order j' by neglecting terms with $j > j'$, provided the higher-order terms are small. In practice, however, insufficient general boundary conditions exist to solve these equations for $j' > 1$ without an iterative approach (as, e.g., in the technique of Leung 1975).

In what follows we treat only the first-order equations, which is equivalent to treating the diffuse field (I_d) in

[2] The somewhat better approximation of the central star as a uniform disk of radius r_* would result in correction factors, C_j, to the L_* terms in eq. (A.2). E.g., $C_0 = 1$, $C_1 = \frac{1}{2}\{1 + 1/[1 + (r^*/r)^2]^{1/2}\}$.

the Eddington approximation. Then the diffuse intensity is $K_0 \sim (1/\rho)S_0$, the diffuse flux per unit area is $[(4\pi)/3]K_1 \sim (1/\rho^2)\,S_1$, and equations (A.3*a*) and (A.3*b*) become

$$S_0' = \frac{1}{\rho}\left(S_0 - \zeta_1 S_1 + \frac{3}{4\pi} g\tilde{\omega}\zeta_d S_*\right) \tag{A.4a}$$

and

$$S_1' = 3\left(\rho^2\eta - \rho\zeta_0 S_0 + \frac{\tilde{\omega}}{4\pi}\,\zeta_d S_*\right), \tag{A.4b}$$

where $g = (\frac{1}{3})p_1$ is the scattering-phase parameter. In addition, we apply the boundary conditions

$$S_1(\rho = \rho_i) = 0 \tag{A.5a}$$

and

$$S_1(\rho = 1) = (\tfrac{3}{2})S_0(\rho = 1)\,, \tag{A.5b}$$

where (A.5*a*) assumes the diffuse flux vanishes at the innermost radius, ρ_i, and (A.5*b*) assumes no flux incident from outside the source. Results described in this paper are based on numerical solutions to equations (A.3*c*) and (A.4) obtained using a fourth-order Runge-Kutta routine and iteration on an initial guess for $S_0(\rho_i)$.

II. ANALYTIC SOLUTIONS

In some simple but interesting cases, one may also obtain analytic solutions to the equations of (A.4), or at least reduce the solution to a problem of quadratures. Consider the opacities to be of the form $\zeta = \zeta^0\rho^{-n}$ and institute a change of variables to $x \equiv \rho^{1-n}$. Then, combining the equations of (A.4), one obtains the single equation

$$S_0'' - \frac{1}{(n-1)^2}\left(3\zeta_0{}^0\zeta_1{}^0 + \frac{n}{x^2}\right)S_0 = -\frac{3}{(n-1)^2}\left[\frac{\tilde{\omega}}{4\pi}\,\zeta_d{}^0(g\cdot\zeta^0 + \zeta_1{}^0)x^{1/(n-1)}S_* + \zeta_1{}^0\eta x^{-(n+1)/(n-1)}\right]. \tag{A.6}$$

For $n = 0$ or 2, the homogeneous solutions to equation (A.6) are the zero- and first-order Riccati-Bessel functions of imaginary argument or, alternatively,

$$S_{0h} = Ae^{\beta x} + Be^{-\beta x} \quad (n = 0)\,;$$

$$S_{0h} = A[e^{\beta x}/(\beta x) - e^{-\beta x}] + B[e^{-\beta x}/(\beta x) + e^{\beta x}] \quad (n = 2)\,,$$

with $\beta^2 = 3\zeta_0{}^0\zeta_1{}^0$. These homogeneous solutions correspond to the solutions obtained if one treats the entire radiation field in the Eddington approximation (see Huang 1969).

As an illustration of the procedure for obtaining the full solution to equation (A.6), consider the $n = 0$ case. The constants A and B are then replaced by

$$A(x) = -\int^x t(z)e^{-\beta z}dz$$

and

$$B(x) = \int^x t(z)e^{\beta z}dz\,, \tag{A.7}$$

with

$$t(z) = \frac{3}{2\beta}\left(z\zeta_1{}^0\eta(z) + \frac{\tilde{\omega}}{16\pi^2 z}\,\zeta_d{}^0(g\zeta^0 + \zeta_1{}^0)e^{-\zeta^0 z}\right).$$

From equation (A.4*a*), one obtains the flux solution

$$S_1 = A\left(\frac{1}{\zeta_1{}^0} - x\beta\right)e^{\beta x} + B\left(\frac{1}{\zeta_1{}^0} + x\beta\right)e^{-\beta x} + \frac{3g\tilde{\omega}}{4\pi}\,\zeta_d{}^0 S_*\,. \tag{A.8}$$

Then, using the boundary conditions (A.5), one finds in the frequently applicable limit $x_i\beta \ll 1$ (with $x_i = \rho_i$)

$$A(x_i) = \frac{3g\tilde{\omega}}{16\pi^2}\left\{\left[\zeta_d{}^0\zeta_1{}^0(T_2 - 1) + T_1\int_{x_i}^1 te^{-\beta z} - T_2\int_{x_i}^1 te^{\beta z}dz\right]\Big/[T_1 - T_2]\right\},$$

$$B(x_i) = \frac{3g\tilde{\omega}}{16\pi^2}\left\{\left[\zeta_d{}^0\zeta_1{}^0(T_1 - 1) + T_1\int_{x_i}^1 te^{-\beta z} - T_2\int_{x_i}^1 te^{\beta z}dz\right]\Big/[T_2 - T_1]\right\}, \tag{A.9}$$

with

$$T_1 = [1 - (\beta + 3/2)\zeta_1{}^0]e^{(\beta+\zeta^0)},$$
$$T_2 = [1 + (\beta - 3/2)\zeta_1{}^0]e^{(-\beta+\zeta^0)} \quad \text{(A.10)}$$

and

$$A(x) = A(x_i) - \int_{x_i}^{x} te^{-\beta z}dz,$$
$$B(x) = B(x_i) + \int_{x_i}^{x} te^{\beta z}dz. \quad \text{(A.11)}$$

When η has a power-law form, the quantities (A.11) may be expressed in terms of exponential integrals or otherwise are easily found by quadratures. In the limit $\mathfrak{F} \to 0$, the solution for η = const. reduces to the simple analytic form given by Jones and Stein (1975). One may apply similar techniques to obtain the $n = 2$ solutions.

REFERENCES

Aannestad, P. A. 1975, *Ap. J.*, **200**, 30.
Andriesse, C. D. 1974, *Astr. and Ap.*, **27**, 257.
Apruzese, J. P. 1974, *Ap. J.*, **188**, 539.
———. 1975, *Ap. J.*, **196**, 761.
———. 1976, *Ap. J.*, in press.
Chandrasekhar, S. 1960, *Radiative Transfer* (New York: Dover).
Dorschner, J. 1968, *Astr. Nach.*, **290**, 171.
———. 1971*a*, *Astr. Nach.*, **292**, 225.
———. 1971*b*, *Astr. Nach.*, **293**, 53.
Dyck, H. M., Lockwood, G. W., and Capps, R. W. 1974, *Ap. J.*, **189**, 89.
Dyck, H. M., and Simon, T. 1975, *Ap. J.*, **195**, 689.
Forrest, W. J., Gillett, F. C., and Stein, W. A. 1975, *Ap. J.*, **195**, 423.
Frogel, J. A., and Hyland, A. R. 1972, *Mém. Soc. Roy. Sci. Liège*, **3**, 111.
Gillett, F. C., Forrest, W. J., Merrill, K. M., Capps, R. W., and Soifer, B. T. 1975, *Ap. J.*, **200**, 609.
Gillett, F. C., Jones, T. W., Merrill, K. M., and Stein, W. A. 1975, *Astr. and Ap.*, **45**, 77.
Gilman, R. C. 1969, *Ap. J.* (*Letters*), **155**, L185.
———. 1972, *Ap. J.*, **178**, 423.
Hackwell, J. A. 1972, *Astr. and Ap.*, **21**, 239.
Hagen, W., Simon, T., and Dyck, H. M. 1975, *Ap. J.* (*Letters*), **201**, L81.
Herbig, G. H. 1970, *Ap. J.*, **162**, 557.
Huang, S. 1969, *Ap. J.*, **157**, 843.
Hummer, D. G., and Rybicki, G. B. 1971, *M.N.R.A.S.*, **152**, 1.
Humphreys, R. M., Strecker, D. W., and Ney, E. P. 1972, *Ap. J.*, **172**, 75.
Hyland, A. R., Becklin, E. E., Frogel, J. A., and Neugebauer, G. 1972, *Astr. and Ap.*, **16**, 204.
Johnson, H. L., Mitchell, R. I., Iriarte, B., and Wisniewski, W. Z. 1966, *Comm. Lunar and Planet. Lab.*, **4**, 99.
Jones, T. W., and Stein, W. A. 1975, *Ap. J.*, **197**, 297.
Knacke, R. F., and Thomson, K. 1973, *Pub. A.S.P.*, **85**, 341.
Kwok, S. 1975, *Ap. J.*, **198**, 583.
Leung, C. M. 1975, *Ap. J.*, **199**, 340.
———. 1976, *Ap. J.*, in press.
Lockwood, G. W. 1970, *Ap. J.* (*Letters*), **160**, L47.
———. 1974, *Ap. J.* (*Letters*), **192**, L113.
Low, F. J., Rieke, G. H., and Armstrong, K. R. 1973, *Ap. J.* (*Letters*), **183**, L105.
Merrill, K. M. 1976, Ph.D. thesis, University of California, San Diego (unpublished).
Merrill, K. M., and Stein, W. A. 1976*a*, *Pub. A.S.P.*, **88**, 294.
———. 1976*b*, *Pub. A.S.P.*, submitted.
Morrison, D., and Simon, T. 1973, *Ap. J.*, **186**, 193.
Neugebauer, G., Becklin, E. E., and Hyland, A. R. 1971, *Ann. Rev. Astr. and Ap.*, **9**, 67.
Neugebauer, G., and Leighton, R. B. 1969, *Two-Micron Sky Survey* (NASA SP-3047, Washington, D.C.)
Pollack, J. B., Toon, O. B., and Khare, B. N. 1973, *Icarus*, **19**, 372.
Salpeter, E. E. 1974*a*, *Ap. J.*, **193**, 579.
———. 1974*b*, *Ap. J.*, **193**, 585.
Simon, T. 1974, *Astr. J.*, **79**, 1054.
Simon, T., and Dyck, H. M. 1975, *Nature*, **253**, 101.
Simon, T., Morrison, D., and Cruikshank, D. P. 1972, *Ap. J.* (*Letters*), **177**, L17.
Strecker, D. W., and Ney, E. P. 1974*a*, *Astr. J.*, **79**, 797.
———. 1974*b*, *Astr. J.*, **79**, 1410.
Taam, R. E., and Schwartz, R. D. 1976, *Ap. J.*, **204**, 842.
Taft, E. A., and Philipp, H. R. 1965, *Phys. Rev.*, **138**, A197.
Treffers, R., and Cohen, M. 1974, *Ap. J.*, **188**, 545.
Vogt, S. S. 1973, *Astr. J.*, **78**, 389.
Walker, R. G., and Price, S. D. 1975, *AFCRL Infrared Sky Survey*, vol. 1, Air Force no. AFCRL-TR-75-0373.
Woolf, N. J. 1973, in *IAU Symposium, No. 52, Interstellar Dust and Related Topics*, ed. J. M. Greenberg and H. C. van de Hulst, p. 485.
Zaikowski, A., and Knacke, R. F. 1975, *Ap. and Space Sci.*, **37**, 3.

T. W. JONES: National Radio Astronomy Observatory, Edgemont Road, Charlottesville, VA 22901

K. M. MERRILL: School of Physics and Astronomy, University of Minnesota, Minneapolis, MN 55455